

Unified Formulation for High-Order Streamline Tracing on Two-Dimensional Unstructured Grids

Ruben Juanes · Sébastien F. Matringe

Received: 19 December 2006 / Revised: 16 January 2008 / Accepted: 7 July 2008 /
Published online: 23 July 2008
© Springer Science+Business Media, LLC 2008

Abstract Accurate streamline tracing and travel time computation are essential ingredients of streamline methods for groundwater transport and petroleum reservoir simulation. In this paper we present a unified formulation for the development of high-order accurate streamline tracing algorithms on unstructured triangular and quadrilateral grids. The main result of this paper is the identification of velocity spaces that are suitable for streamline tracing. The essential requirement is that the divergence-free part of the velocity must induce a stream function. We recognize several classes of velocity spaces satisfying this requirement from the theory of mixed finite element methods and, for each class, we obtain the precise functional form of the stream function. Not surprisingly, the most widely used tracing algorithm (Pollock's method) emanates in fact from the lowest-order admissible velocity approximation. Therefore, we provide a sound theoretical justification for the low-order algorithms currently in use, and we show how to achieve higher-order accuracy both in the streamline tracing and the travel time computation.

Keywords Streamline methods · Streamline tracing · Mixed finite elements · Stream function · Darcy flow · Groundwater · Petroleum reservoir simulation

1 Introduction

Streamline methods have re-emerged in recent years as an attractive alternative to traditional petroleum reservoir simulation based on finite difference methods [4, 6, 23]. The equations

R. Juanes (✉)
Dept. of Civil and Environmental Engineering, Massachusetts Institute of Technology,
77 Massachusetts Ave, Room 48-319, Cambridge, MA 02139, USA
e-mail: juanes@mit.edu

S.F. Matringe
Dept. of Energy Resources Engineering, Stanford University, 65 Green Earth Sciences Building,
Stanford, CA 94305, USA
e-mail: matringe@stanford.edu

governing the flow of fluids in the subsurface (oil and gas reservoirs, confined aquifers, vadose zone, etc.) are mass conservation equations for a number of chemical species, coupled with constitutive relations defining the flux of the different phases and algebraic equations describing phase transitions and physical constraints [2, 5]. In many cases, it is possible to formulate the problem in terms of a single “pressure” equation (or flow equation) describing an overall mass balance, and “component” equations (or transport equations) governing the differential displacement of each component [2, 13, 14]. In the streamline approach, the three-dimensional transport equations are decoupled into a set of one-dimensional problems along streamlines. Streamlines are traced using the velocity field obtained from the solution of the pressure equation. In this way, streamline methods exploit the markedly different character of the essentially elliptic pressure equation, and the essentially hyperbolic system of transport equations.

Current streamline methods employ a low-order velocity field proposed by Pollock [33] as a basis for streamline tracing. It has been shown, however, that low-order accurate streamline tracing may lead to large errors in both streamline location and in the travel time of particles along streamlines, concluding that a higher-order method is desirable [25–27, 30]. Accurate streamline tracing is also often needed for the evaluation of travel times in stochastic subsurface simulation [19], and for computer-aided visualization [18].

Most subsurface-flow streamline simulators are based on the use of Pollock’s method, which is valid only for rectangular, Cartesian grids. An extension of Pollock’s tracing algorithm to distorted quadrilateral grids was first proposed (in the groundwater hydrology literature) by Cordes and Kinzelbach [15]. They presented a generalization in the context of nodal-based finite element models, which requires a flux reconstruction step to obtain continuous velocity fields. Shortcomings associated with the use of nodal-based finite element methods (such as lack of mass conservation at the element level, discontinuous velocity fields, incorrect averaging in the presence of heterogeneity, and nonphysical streamlines) have been pointed out by several authors [1, 16, 17, 31]. Such problems are not present in the finite difference method or the mixed finite element method—in which the pressure and the velocity are solved for simultaneously. For triangular grids, the tracing of streamlines is straightforward, and mixed finite element methods have been shown to produce physical streamlines even on very coarse grids [17, 22, 31]. Recently, extensions of the streamline tracing algorithms to unstructured triangular and quadrilateral grids have been proposed in the framework of flux-continuous finite volume methods [20, 21, 34]. The essence of these extensions is the use of Pollock’s method on the reference element (unit square), together with a proper transformation of the flux from the spatial configuration to the reference configuration known as the Piola transform [9].

All the developments mentioned above are restricted, however, to the lowest-order accurate description of the velocity field. The aim of this paper is to give a rather general and consistent approach for the development of high-order accurate tracing algorithms on unstructured grids—both triangular and quadrilateral. The basic ingredient of the proposed approach is the proper definition of the space where the velocity is sought. Thus, one of the main objectives of this paper is to provide a unified framework for the definition of appropriate velocity spaces. In doing so, we present a sound theoretical justification for the low-order tracing algorithms currently in use, and we show how to extend the streamline tracing to achieve higher order accuracy. The fundamental observation is that the velocity field used as a basis for streamline tracing (or, more precisely, the divergence-free part of it) should induce a stream function. The existence of a stream function guarantees a certain well-posedness of the velocity field. Since the stream function is constant along a streamline, knowledge of the stream function can also lead to highly efficient tracing algorithms. The main results of this paper may be summarized as follows:

1. We recognize that a large class of velocity spaces inducing a stream function can be identified from the theory of mixed finite element methods.
2. We obtain the precise *functional form* of the stream function for each velocity space. In addition to its immediate practical implications, this result may be seen as a *constructive* proof of the existence of the stream function for a large class of mixed finite element spaces.

While the theory is general, we have limited our applications to velocity spaces that are compatible with a piecewise-constant pressure space, therefore limiting the order of approximation of the velocity field (first-order for RT_0 [35] and second-order for BDM_1 [10]). The restriction to piecewise constant pressure is driven by practical considerations of flow through porous media, in that mixed finite element methods can be linked to commonly-used finite volume methods [12, 28, 29, 36–38].

In Sect. 2 we explain the overall strategy for streamline tracing. In Sect. 3 we pose the model problem in mixed variational form, we identify appropriate velocity spaces from the theory of mixed finite elements, and we revisit some of their relevant properties (in particular, the existence of a stream function). Section 4 is devoted to the derivation of the functional form of the stream function for each of the velocity spaces introduced. A discussion on the computation of the travel time, and its exact expression, is included in Sect. 5. In Sect. 6 we present some representative numerical simulations that illustrate the performance of the proposed tracing algorithm for different choices of velocity spaces on a variety of grids. In Sect. 7 we make some concluding remarks, and anticipate ongoing and future work.

2 Strategy for Streamline Tracing

The general strategy is to identify streamlines as loci of constant values of the stream function. Such procedure relies on the existence of the stream function, and the ability to compute it. Obviously, a stream function will not exist for an arbitrary velocity field. In the next sections, we identify velocity spaces that guarantee the existence of a stream function, and we obtain its precise functional form.

The domain is discretized into triangular or quadrilateral elements, and tracing is performed on individual elements. The velocity field is mapped from the real space to a reference element by means of the Piola transform, which allows to preserve the normal components of the flux across the element edges (and thus guarantees local mass conservation). Once the functional form of the stream function is known, a streamline is traced on a particular element by evaluating the stream function at the entry point, and determining the loci where the stream function is constant, and equal to its entry-point value. One is often interested only on the *exit point* of the streamline (for that specific element), and the *travel time* required to traverse the element. The exit point can be easily identified because the reference element has a very simple geometry. The travel time or time-of-flight, which involves the evaluation of an integral along the streamline, can then be calculated numerically or, for simple cases, analytically (see Sect. 5).

The tracing procedure just described is applicable only where a stream function exists. In particular, this implies that the velocity must be divergence-free and, consequently, the source term in the mass balance equation must be identically zero. This is typically the case in reservoir simulation and many other problems in fluid mechanics, where the source term is concentrated along part of the boundary, or on a few source/sink points (injection and production wells). Boundary sources do not introduce any difficulty, as the boundary

flux is known (either *a priori* or as a result of a numerical simulation). In the case of point sources, streamline tracing is not performed inside the well blocks. This limitation is of minor concern for two reasons: (1) one should not expect high accuracy in the streamline predictions near a point source anyway, because the discretization level is insufficient to resolve the flow field; and (2) since it is a region of high velocity, the time-of-flight along the well block is insignificant compared with the travel time along the entire streamline.

3 Velocity Spaces

The objective of this section is to give a concise summary and a unified view of proper velocity spaces that are suitable for streamline tracing. More specifically, a number of velocity spaces are identified from the theory of mixed finite element methods.

First, we introduce the mixed variational form of the continuum problem, and introduce the proper space where the velocity is defined. Then, we revisit several classes of mixed finite elements that provide a successful discrete approximation to the continuum problem. They all share the following common features:

1. They are conforming, that is, the velocity spaces are finite-dimensional subspaces of $H(\text{div})$.
2. They satisfy the discrete inf-sup condition [3, 8], required for stability and convergence of the mixed finite element method.
3. They are locally mass conservative, that is, the numerical scheme satisfies mass conservation at the element level exactly.
4. They induce a stream function.

For each class of velocity spaces, we give their fundamental properties, and recall important results regarding the existence of a stream function.

3.1 Mixed Variational Formulation

In this paper, we shall use the following model pressure equation:

$$\text{div } \mathbf{u} = f \quad \text{in } \Omega \in \mathbb{R}^2, \tag{1}$$

where f is the source term, and \mathbf{u} is the total velocity given by Darcy’s law:

$$\mathbf{u} = -\mathbf{k}\nabla p. \tag{2}$$

The symbol \mathbf{k} is the permeability tensor and p is the pressure. In a more general setting (multiphase flow problems including gravity effects) \mathbf{k} is the total mobility tensor, and p is the flow potential. The permeability tensor is symmetric and positive definite. The components of \mathbf{k} are assumed to be bounded, but they may be highly discontinuous and display large anisotropy ratios. The pressure equation is supplemented with the following boundary conditions:

$$p = \bar{p} \quad \text{on } \Gamma_p, \tag{3}$$

$$\mathbf{u} \cdot \mathbf{n} = \bar{u} \quad \text{on } \Gamma_u, \tag{4}$$

where $\Gamma_p \cap \Gamma_u = \emptyset$, $\Gamma_p \cup \Gamma_u = \partial\Omega$, and \mathbf{n} is the outward unit normal to the boundary. Without loss of generality (see, e.g. [9, Sect. IV.1]), we may take a homogeneous Neumann boundary condition:

$$\bar{u} = 0 \quad \text{on } \Gamma_u. \tag{5}$$

Let us introduce the following functional spaces:

$$L^2(\Omega) = \left\{ q : \int_{\Omega} |q|^2 \, d\Omega = \|q\|_{L^2(\Omega)}^2 < +\infty \right\}, \tag{6}$$

$$H(\text{div}, \Omega) = \{ \mathbf{v} : \mathbf{v} \in (L^2(\Omega))^2, \text{div } \mathbf{v} \in L^2(\Omega) \}. \tag{7}$$

The space $L^2(\Omega)$ is the usual Sobolev space of square integrable functions in Ω . The space $H(\text{div}, \Omega)$ is defined such that vectors belonging to this space admit a well-defined normal trace on $\partial\Omega$ [9, Sect. III.1.1]. We will also make use of the following space:

$$H_{0,u}(\text{div}, \Omega) = \{ \mathbf{v} : \mathbf{v} \in H(\text{div}, \Omega), \mathbf{v} \cdot \mathbf{n} = 0 \text{ on } \Gamma_u \}. \tag{8}$$

Remark The condition $\mathbf{v} \cdot \mathbf{n} = 0$ on Γ_u appearing in (8) should be understood in a weak sense. See [9, Sect. III.1.1] for a precise definition.

Under some regularity conditions on the source function f and the boundary conditions \bar{p} , the problem given by (1)–(5) can be expressed in mixed variational form as follows:

Find $(\mathbf{u}, p) \in H_{0,u}(\text{div}, \Omega) \times L^2(\Omega)$ such that

$$\int_{\Omega} \mathbf{v} \cdot \mathbf{k}^{-1} \mathbf{u} \, d\Omega - \int_{\Omega} \text{div } \mathbf{v} p \, d\Omega = - \int_{\Gamma_p} \mathbf{v} \cdot \mathbf{n} \bar{p} \, d\Gamma \quad \forall \mathbf{v} \in H_{0,u}(\text{div}, \Omega), \tag{9}$$

$$\int_{\Omega} q \, \text{div } \mathbf{u} \, d\Omega = \int_{\Omega} q f \, d\Omega \quad \forall q \in L^2(\Omega). \tag{10}$$

Employing the usual inner-product and duality notation,

$$(q, p) \equiv (q, p)_{L^2(\Omega)} := \int_{\Omega} q p \, d\Omega, \quad q, p \in L^2(\Omega), \tag{11}$$

$$(\mathbf{v}, \mathbf{u}) \equiv (\mathbf{v}, \mathbf{u})_{H(\text{div}, \Omega)} := \int_{\Omega} \mathbf{v} \cdot \mathbf{u} \, d\Omega, \quad \mathbf{v}, \mathbf{u} \in H(\text{div}, \Omega), \tag{12}$$

$$\langle \bar{u}, \bar{p} \rangle_{\Gamma} := \int_{\Gamma} \bar{u} \bar{p} \, d\Gamma, \quad \bar{u} \in H^{1/2}(\Gamma), \bar{p} \in H^{-1/2}(\Gamma), \tag{13}$$

and defining the bilinear form

$$a(\mathbf{v}, \mathbf{u}) := (\mathbf{v}, \mathbf{k}^{-1} \mathbf{u}), \tag{14}$$

(9)–(10) are written as follows:

$$a(\mathbf{v}, \mathbf{u}) - (\text{div } \mathbf{v}, p) = -\langle \mathbf{v} \cdot \mathbf{n}, \bar{p} \rangle_{\Gamma_p} \quad \forall \mathbf{v} \in H_{0,u}(\text{div}, \Omega), \tag{15}$$

$$(q, \text{div } \mathbf{u}) = (q, f) \quad \forall q \in L^2(\Omega). \tag{16}$$

It is well known that the problem (15)–(16) has a unique solution [9]. This weak formulation of the problem provides the basis for the mixed finite element method. Let $V_h \subset H(\text{div}, \Omega)$,

and $Q_h \subset L^2(\Omega)$ be finite dimensional subspaces of the corresponding continuum spaces, and define:

$$V_{h,0} = \{\mathbf{v} : \mathbf{v} \in V_h, \mathbf{v} \cdot \mathbf{n} = 0 \text{ on } \Gamma_u\}. \tag{17}$$

The discrete mixed finite element approximation of (15)–(16) reads:

Find $(\mathbf{u}_h, p_h) \in V_{h,0} \times Q_h$ such that

$$a(\mathbf{v}_h, \mathbf{u}_h) - (\operatorname{div} \mathbf{v}_h, p_h) = -(\mathbf{v}_h \cdot \mathbf{n}, \bar{p})_{\Gamma_p} \quad \forall \mathbf{v}_h \in V_{h,0}, \tag{18}$$

$$(q_h, \operatorname{div} \mathbf{u}_h) = (q_h, f) \quad \forall q_h \in Q_h. \tag{19}$$

The spaces V_h and Q_h cannot be chosen independently. They must satisfy two key conditions in order to obtain a convergent approximation [7, 9]: a standard coercivity condition, and the discrete inf-sup condition [3, 8].

The numerical solution of (18)–(19) invariably involves a partition \mathcal{T}_h of the domain Ω into nonoverlapping elements K_i (triangles or quadrilaterals), $\Omega = \bigcup_{i=1}^m K_i$. We denote by \mathcal{E}_h the set of all element edges of \mathcal{T}_h . Discrete approximations of $H(\operatorname{div}, \Omega)$ make use of the following functional space:

$$Y(\Omega, \mathcal{T}_h) = \{\mathbf{v} : \mathbf{v} \in (L^2(\Omega))^2, \mathbf{v}|_{K_i} \in H(\operatorname{div}, K_i) \forall K_i \in \mathcal{T}_h\}. \tag{20}$$

It can be shown that functions of $Y(\Omega, \mathcal{T}_h)$ belong to $H(\operatorname{div}, \Omega)$ if their normal traces are continuous (in a weak sense) at the element interfaces [9, Sect. III.1.2]. This fact suggests how discrete approximations of $H(\operatorname{div}, \Omega)$ are constructed: the functional space is chosen to belong to $H(\operatorname{div})$ inside each element, and the requirement of continuity of the normal trace is achieved by a proper selection of the degrees of freedom.

Discrete subspaces of $H(\operatorname{div}, K)$ are usually constructed through a *reference element* \hat{K} and a change of coordinates from physical space to reference space. Following [9], we recall here some of the elementary facts regarding this transformation. Let $\hat{K} \subset \mathbb{R}^2$ be a reference element, and $\partial \hat{K}$ be its boundary. Let φ be a smooth, invertible mapping that maps the reference element \hat{K} onto the element K in physical space:

$$\begin{aligned} \varphi : \mathbb{R}^2 &\longrightarrow \mathbb{R}^2, \\ \hat{\mathbf{x}} \in \hat{K} &\mapsto \mathbf{x} = \varphi(\hat{\mathbf{x}}) \in K. \end{aligned} \tag{21}$$

We assume that the Jacobian matrix $\mathbf{D}(\hat{\mathbf{x}})$ is invertible for any $\hat{\mathbf{x}} \in \hat{K}$, and we define the Jacobian of the transformation $J(\hat{\mathbf{x}}) = \det \mathbf{D}(\hat{\mathbf{x}})$, assumed to be bounded away from zero. Let $\hat{q}(\hat{\mathbf{x}})$ be a scalar function on \hat{K} , we define the function $q(\mathbf{x})$ on K by:

$$q(\mathbf{x}) = \mathcal{F}(\hat{q})(\mathbf{x}) = \hat{q}(\hat{\mathbf{x}}), \quad \text{with } \mathbf{x} = \varphi(\hat{\mathbf{x}}). \tag{22}$$

The mapping \mathcal{F} is an isomorphism from $L^2(\hat{K})$ onto $L^2(K)$. Such transformation is inappropriate for building approximations of $H(\operatorname{div}, \Omega)$, because it does not preserve normal components and does not map $H(\operatorname{div}, \hat{K})$ onto $H(\operatorname{div}, K)$. Instead, the vector function $\hat{\mathbf{v}}(\hat{\mathbf{x}}) \in (L^2(\hat{K}))^2$ is transformed according to the *Piola transform* [9, 24]:

$$\mathbf{v}(\mathbf{x}) = \mathcal{P}(\hat{\mathbf{v}})(\mathbf{x}) = \frac{1}{J(\hat{\mathbf{x}})} \mathbf{D}(\hat{\mathbf{x}}) \hat{\mathbf{v}}(\hat{\mathbf{x}}), \quad \text{with } \mathbf{x} = \varphi(\hat{\mathbf{x}}). \tag{23}$$

The mapping \mathcal{P} preserves the normal trace and, moreover, is an isomorphism of $H(\operatorname{div}, \hat{K})$ onto $H(\operatorname{div}, K)$. These properties of the Piola transform allow one to define subspaces of $H(\operatorname{div}, K)$ through the reference element \hat{K} .

Let the space $M_k(K)$ denote a finite-dimensional approximation of $H(\operatorname{div}, K)$. This space must be designed such that the degrees of freedom ensure continuity of normal traces at the element interfaces. Also, let $D_k(K)$ denote the space of divergences of vectors in $M_k(K)$:

$$D_k(K) := \operatorname{div}(M_k(K)). \tag{24}$$

One can then define a finite-dimensional space that approximates $H(\operatorname{div}, \Omega)$:

$$V_h \equiv M_k(\Omega, \mathcal{T}_h) = \{\mathbf{v} \in H(\operatorname{div}, \Omega), \mathbf{v}|_{K_i} \in M_k(K_i) \forall K_i \in \mathcal{T}_h\}. \tag{25}$$

The space approximating $L^2(\Omega)$ must be

$$Q_h \equiv L^0(D_k, \mathcal{T}_h) = \{q \in L^2(\Omega), q|_{K_i} \in D_k(K_i) \forall K_i \in \mathcal{T}_h\}. \tag{26}$$

For affine elements (triangles), one has the imbedding $\operatorname{div} V_h \subseteq Q_h$. This is not the case, however, for general quadrilateral elements, which makes some of the approximation results much more difficult to obtain [9].

In what follows, we present several well-known classes of velocity spaces $M_k(K)$ that lead to convergent approximations of the mixed variational problem.

3.2 Velocity Spaces on Triangles

We revisit two well-known classes of mixed finite elements, which provide conforming approximations to $H(\operatorname{div})$. We will define them on the reference triangle \hat{K} . The mapping from reference to physical space for triangular elements is shown in Fig. 1. The map φ is given by the isoparametric mapping:

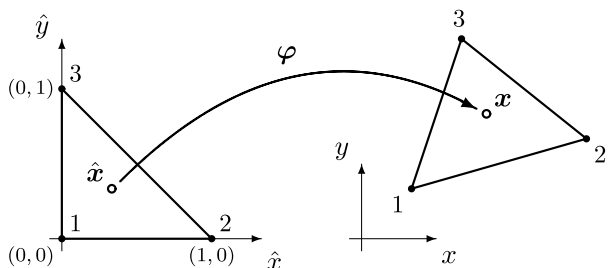
$$\mathbf{x} = \varphi(\hat{\mathbf{x}}) = \sum_{a=1}^3 N_a(\hat{\mathbf{x}})\mathbf{x}_a, \tag{27}$$

where \mathbf{x}_a are the nodal coordinates (in physical space), and N_a are the usual linear finite element hat functions:

$$N_1(\hat{x}, \hat{y}) = 1 - \hat{x} - \hat{y}, \quad N_2(\hat{x}, \hat{y}) = \hat{x}, \quad N_3(\hat{x}, \hat{y}) = \hat{y}. \tag{28}$$

The Jacobian matrix \mathbf{D} is constant and, therefore, the mapping is affine. In the remainder of this section, we shall work on the reference configuration exclusively. We abuse notation and drop the tilde, but still denote quantities defined on the reference element.

Fig. 1 Mapping of the reference element onto physical space for triangular elements



3.2.1 Raviart-Thomas Spaces

Some of the first mixed finite element spaces for the approximation of $H(\text{div})$ were introduced by Raviart and Thomas [35]. The extension to three dimensions was presented in [32]. Following [9, Sect. III.2.1], we introduce some notation. We denote by $P_k(K)$ the space of polynomials on K of degree less than or equal to k :

$$P_k(K) = \left\{ p(x, y) : p(x, y) = \sum_{j=0}^k \sum_{i=0}^j a_{j-i,i} x^{j-i} y^i \right\}. \tag{29}$$

The dimension of $P_k(K)$ is $\frac{1}{2}(k + 1)(k + 2)$. We shall also use the space

$$P_{k_1,k_2}(K) = \left\{ p(x, y) : p(x, y) = \sum_{i=0}^{k_1} \sum_{j=0}^{k_2} a_{i,j} x^i y^j \right\}, \tag{30}$$

whose dimension is $(k_1 + 1)(k_2 + 1)$. We denote by $Q_k(K)$ the space:

$$Q_k(K) = P_{k,k}(K). \tag{31}$$

We will also make use of the following space of polynomials defined on the edges:

$$R_k(\partial K) = \{q : q \in L^2(\partial K), q|_{e_i} \in P_k(e_i) \forall e_i\}. \tag{32}$$

Functions in $R_k(\partial K)$ do not have to be continuous at the vertices and, for triangles, the dimension of the space is $3(k + 1)$.

We now give the definition and a few relevant properties of the Raviart-Thomas class of velocity spaces. Let K be the reference triangle in Fig. 1. We define, for $k \geq 0$,

$$\begin{aligned} RT_k(K) &= (P_k(K))^2 \oplus \mathbf{x}P_k(K) \\ &= \left\{ \mathbf{v}(x, y) : \begin{bmatrix} v^x(x, y) \\ v^y(x, y) \end{bmatrix} = \sum_{j=0}^k \sum_{i=0}^j \begin{bmatrix} a_{j-i,i}^x \\ a_{j-i,i}^y \end{bmatrix} x^{j-i} y^i + \left(\sum_{i=0}^k b_{k-i,i} x^{k-i} y^i \right) \begin{bmatrix} x \\ y \end{bmatrix} \right\}. \end{aligned} \tag{33}$$

The dimension of $RT_k(K)$ is $(k + 1)(k + 3)$. It can be shown that $RT_k(K)$ is fully characterized by the following degrees of freedom:

- the moments of order up to k of $\mathbf{v} \cdot \mathbf{n}$ on the edges of K ;
- the moments of order up to $k - 1$ of \mathbf{v} on K .

Obviously, one has that

$$\dim RT_k(K) = \dim R_k(\partial K) + \dim(P_{k-1}(K))^2. \tag{34}$$

The subspace of divergence-free functions belonging to $RT_k(K)$ will play an essential role:

$$RT_k^0(K) = \{\mathbf{v} \in RT_k(K) : \text{div } \mathbf{v} = 0\}. \tag{35}$$

It is clear that if $\mathbf{v} \in RT_k(K)$, then $\operatorname{div} \mathbf{u} \in P_k(K)$, so the divergence-free condition reduces the number of degrees of freedom by $\frac{1}{2}(k+1)(k+2)$. Therefore,

$$\dim RT_k^0 = \frac{1}{2}(k+1)(k+4) = \dim P_{k+1}(K) - 1. \tag{36}$$

This fact is used in [9] to state the following fundamental result:

Any $\mathbf{v}_0 \in RT_k^0(K)$ is the curl of a stream function $\psi \in P_{k+1}(K)$, that is,

$$v_0^x = \frac{\partial \psi}{\partial y}, \quad v_0^y = -\frac{\partial \psi}{\partial x}. \tag{37}$$

3.2.2 Brezzi-Douglas-Marini Spaces

Another class of velocity spaces approximating $H(\operatorname{div}, K)$ was presented in [10], and extended to three dimensions in [11]. Let K be the reference triangle in Fig. 1. We define, for $k \geq 1$,

$$\begin{aligned} BDM_k(K) &= (P_k(K))^2 \\ &= \left\{ \mathbf{v}(x, y) : \begin{bmatrix} v^x(x, y) \\ v^y(x, y) \end{bmatrix} = \sum_{j=0}^k \sum_{i=0}^j \begin{bmatrix} a_{j-i,i}^x \\ a_{j-i,i}^y \end{bmatrix} x^{j-i} y^i \right\}. \end{aligned} \tag{38}$$

The dimension of $BDM_k(K)$ is $(k+1)(k+2)$. The degrees of freedom can be chosen from a basis of $R_k(\partial K)$, $P_{k-1}(K)$ and the space

$$\Phi_k(K) = \{ \boldsymbol{\phi}_k \in (P_k(K))^2 : \operatorname{div} \boldsymbol{\phi}_k = 0, \boldsymbol{\phi}_k \cdot \mathbf{n}|_{\partial K} = 0 \}. \tag{39}$$

Indeed, one has that

$$\dim BDM_k(K) = \dim R_k(\partial K) + (\dim P_{k-1}(K) - 1) + \dim \Phi_k(K). \tag{40}$$

In the same way as for Raviart-Thomas spaces, we can define the subspace of divergence-free functions:

$$BDM_k^0(K) = \{ \mathbf{v} \in BDM_k(K) : \operatorname{div} \mathbf{v} = 0 \}. \tag{41}$$

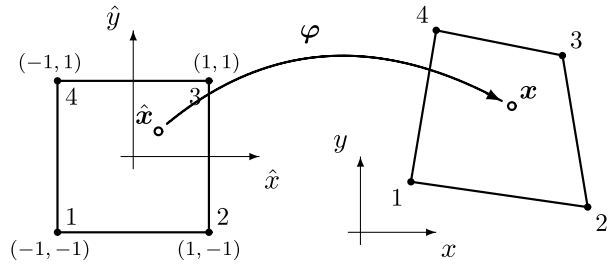
It is easy to show that $BDM_k(K)$ and $RT_k(K)$ contain the same divergence-free functions and, therefore, $BDM_k^0(K) \equiv RT_k^0(K)$. It then follows that any $\mathbf{v}_0 \in BDM_k^0(K)$ is the curl of a stream function.

3.3 Velocity Spaces on Rectangles

We now discuss two classes of velocity spaces approximating $H(\operatorname{div}, \hat{K})$ on the reference element (unit square). The mapping from reference to physical space for quadrilateral elements is depicted in Fig. 2. The map $\boldsymbol{\varphi}$ is again given by the isoparametric mapping:

$$\mathbf{x} = \boldsymbol{\varphi}(\hat{\mathbf{x}}) = \sum_{a=1}^4 N_a(\hat{\mathbf{x}}) \mathbf{x}_a, \tag{42}$$

Fig. 2 Mapping of the reference element onto physical space for quadrilateral elements



where \mathbf{x}_a are the nodal coordinates (in physical space), and N_a are the usual bilinear finite element hat functions:

$$\begin{aligned}
 N_1(\hat{x}, \hat{y}) &= \frac{1}{4}(1 - \hat{x})(1 - \hat{y}), & N_2(\hat{x}, \hat{y}) &= \frac{1}{4}(1 + \hat{x})(1 - \hat{y}), \\
 N_3(\hat{x}, \hat{y}) &= \frac{1}{4}(1 + \hat{x})(1 + \hat{y}), & N_4(\hat{x}, \hat{y}) &= \frac{1}{4}(1 - \hat{x})(1 + \hat{y}).
 \end{aligned}
 \tag{43}$$

As opposed to the case of triangular elements, the Jacobian matrix $\mathbf{D}(\hat{\mathbf{x}})$ is *not* constant and, therefore, the mapping is not affine. Once again, we shall drop the tilde but understand that the spaces are defined on the reference element.

3.3.1 Raviart-Thomas Spaces

This class of velocity spaces on rectangles was introduced in [35] and extended to the three-dimensional case in [32]. Let K be the reference square $[-1, 1] \times [-1, 1]$ in Fig. 2. We define, for $k \geq 0$,

$$\begin{aligned}
 RT_{[k]}(K) &= (\mathcal{Q}_k(K))^2 \oplus \mathbf{x}\mathcal{Q}_k(K) = P_{k+1,k}(K) \times P_{k,k+1}(K) \\
 &= \left\{ \mathbf{v}(x, y) : \begin{bmatrix} v^x(x, y) \\ v^y(x, y) \end{bmatrix} = \begin{bmatrix} \sum_{i=0}^{k+1} \sum_{j=0}^k a_{i,j}^x x^i y^j \\ \sum_{i=0}^k \sum_{j=0}^{k+1} a_{i,j}^y x^i y^j \end{bmatrix} \right\}.
 \end{aligned}
 \tag{44}$$

The dimension of $RT_{[k]}(K)$ is $2(k + 1)(k + 2)$. The degrees of freedom can be chosen from a basis of the spaces $R_k(\partial K)$ and

$$\Psi_k(K) = P_{k-1,k}(K) \times P_{k,k-1}(K).
 \tag{45}$$

Indeed, one has

$$\dim RT_{[k]}(K) = \dim R_k(\partial K) + \dim \Psi_k(K).
 \tag{46}$$

We can define, as for the case of triangles, the subspace of divergence-free functions:

$$RT_{[k]}^0(K) = \{ \mathbf{v} \in RT_{[k]}(K) : \operatorname{div} \mathbf{v} = 0 \}.
 \tag{47}$$

If $\mathbf{v} \in RT_{[k]}(K)$, then $\operatorname{div} \mathbf{v} \in \mathcal{Q}_k(K)$. Therefore,

$$\dim RT_{[k]}^0(K) = \dim RT_{[k]}(K) - \dim \mathcal{Q}_k(K) = (k + 1)(k + 3) - (k + 1) = \dim \mathcal{Q}_{k+1} - 1.
 \tag{48}$$

This fact is used in [9] to state the following fundamental result:

If $\mathbf{v}_0 \in RT_{[k]}^0(K)$, there exists a stream function $\psi \in \mathcal{Q}_{k+1}(K)$ such that $\mathbf{v}_0 = \operatorname{curl} \psi$.

3.3.2 Brezzi-Douglas-Marini Spaces

Here we review the class of velocity spaces for the approximation of $H(\text{div}, K)$ on rectangles introduced in [10], later extended to the three-dimensional case in [11]. Again, let K be the reference square element. For $k \geq 1$ we define

$$BDM_{[k]}(K) = (P_k(K))^2 \oplus \text{curl}(x^{k+1}y) \oplus \text{curl}(xy^{k+1}). \tag{49}$$

The dimension of $BDM_{[k]}(K)$ is $(k + 1)(k + 2) + 2$. The degrees of freedom can be taken from a basis of $R_k(\partial K)$ and $(P_{k-2}(K))^2$. Indeed,

$$\dim BDM_{[k]}(K) = \dim R_k(\partial K) + \dim(P_{k-2}(K))^2. \tag{50}$$

We define the subspace of divergence-free functions:

$$BDM_{[k]}^0(K) = \{\mathbf{v} \in BDM_{[k]}(K) : \text{div } \mathbf{v} = 0\}. \tag{51}$$

Since the curl-terms in the definition of $BDM_{[k]}(K)$ have zero divergence, one has that $\text{div}(BDM_{[k]}(K)) = P_{k-1}(K)$. It follows that

$$\begin{aligned} \dim BDM_{[k]}^0(K) &= \dim BDM_{[k]}(K) - \dim P_{k-1}(K) \\ &= \frac{1}{2}(k + 1)(k + 4) + 2 = (\dim P_{k+1}(K) - 1) + 2. \end{aligned} \tag{52}$$

Based on the results presented in the previous sections, one concludes that

For any $\mathbf{v}_0 \in BDM_{[k]}^0(K)$, there exists a stream function $\psi \in P_{k+1}(K) \oplus x^{k+1}y \oplus xy^{k+1}$ such that $\mathbf{v}_0 = \text{curl } \psi$.

4 Stream Functions

In Sect. 3 we have identified several classes of velocity spaces with the following important property: the functions belonging to their corresponding zero-divergence subspaces induce a stream function. In this section, we determine the *functional form* of the stream function for each of the velocity spaces presented. This constitutes the main result of the paper, and is an essential ingredient of the streamline tracing procedure outlined in Sect. 2.

The derivation of the stream function follows the same steps in all cases. Let $M_k(K)$ be any of the approximations to $H(\text{div}, K)$ introduced in Sect. 3, and $M_k^0(K)$ be its corresponding subspace of divergence-free functions. One starts with the general functional form of a function $\mathbf{v} = (v^x, v^y) \in M_k(K)$. A set of algebraic equations is identified from the condition that $\text{div } \mathbf{v} = 0$, so that $\mathbf{v} \in M_k^0(K)$. The stream function ψ can then be obtained by direct integration of the following two equations:

$$\frac{\partial \psi}{\partial x} = -v^y \quad \longrightarrow \quad \psi(x, y) = \psi^x(x, y) + g(y), \tag{53}$$

$$\frac{\partial \psi}{\partial y} = v^x \quad \longrightarrow \quad \psi(x, y) = \psi^y(x, y) + f(x). \tag{54}$$

A stream function indeed exists if one can express:

$$\psi^x(x, y) - \psi^y(x, y) = f(x) - g(y). \tag{55}$$

Identification of terms allows one to determine the functions $f(x)$ and $g(y)$ and, ultimately, the form of the stream function $\psi(x, y)$.

4.1 Stream Functions on Triangles

4.1.1 Raviart-Thomas Spaces

We start with the Raviart-Thomas velocity spaces on triangles. Recall that

$$RT_k(K) = (P_k(K))^2 \oplus \mathbf{x}P_k(K). \tag{56}$$

For convenience, we express this space as the direct sum of spaces of homogeneous polynomials:

$$RT_k(K) = \bigoplus_{j=0}^k (\tilde{P}_j(K))^2 \oplus \mathbf{x}\tilde{P}_k(K), \tag{57}$$

where

$$(\tilde{P}_j(K))^2 = \left\{ \tilde{\mathbf{v}}_j(x, y) : \begin{bmatrix} \tilde{v}_j^x(x, y) \\ \tilde{v}_j^y(x, y) \end{bmatrix} = \sum_{l=0}^j \begin{bmatrix} a_{j-l,l}^x \\ a_{j-l,l}^y \end{bmatrix} x^{j-l} y^l \right\}, \tag{58}$$

and

$$\mathbf{x}\tilde{P}_k(K) = \left\{ \tilde{\mathbf{v}}_{k+1}(x, y) : \begin{bmatrix} \tilde{v}_{k+1}^x(x, y) \\ \tilde{v}_{k+1}^y(x, y) \end{bmatrix} = \left(\sum_{l=0}^k b_{k-l,l} x^{k-l} y^l \right) \begin{bmatrix} x \\ y \end{bmatrix} \right\}. \tag{59}$$

The condition $\text{div } \mathbf{v} = 0$ implies $\text{div } \tilde{\mathbf{v}}_j = 0$ for $j = 0, \dots, k$ and $\text{div } \tilde{\mathbf{v}}_{k+1} = 0$. This last condition implies, in turn,

$$\text{div } \tilde{\mathbf{v}}_{k+1} = \sum_{l=0}^k [(k-l+1)b_{k-l,l}x^{k-l}y^l + (l+1)b_{k-l,l}x^{k-l}y^l] = 0. \tag{60}$$

Since $k \geq 0$, the equation above can only be satisfied if all $b_{k-l,l} = 0$ for $l = 0, \dots, k$. Now, the condition $\text{div } \tilde{\mathbf{v}}_j = 0$ for $j \geq 1$ reads

$$\text{div } \tilde{\mathbf{v}}_j = \sum_{l=0}^j [(j-l)a_{j-l,l}^x x^{j-l-1} y^l + l a_{j-l,l}^y x^{j-l} y^{l-1}] = 0. \tag{61}$$

Rearranging the indices, the equation above can be written as follows:

$$\sum_{l=0}^j (j-l)a_{j-l,l}^x x^{j-l-1} y^l = - \sum_{l=-1}^{j-1} (l+1)a_{j-l-1,l+1}^y x^{j-l-1} y^l. \tag{62}$$

For this relation to hold for any (x, y) , the following conditions must be satisfied:

$$(j-l)a_{j-l,l}^x = -(l+1)a_{j-l-1,l+1}^y \quad \text{for } l = 0, \dots, j-1. \tag{63}$$

We now use the equations defining the stream function of $\tilde{\mathbf{v}}_j \in (\tilde{P}_j(K))^2$:

$$\frac{\partial \tilde{\psi}_j}{\partial x} = -\tilde{v}_j^y(x, y), \quad \frac{\partial \tilde{\psi}_j}{\partial y} = \tilde{v}_j^x(x, y). \tag{64}$$

Integrating the first equation in (64), we obtain

$$\tilde{\psi}_j = - \int \tilde{v}_j^y(x, y)dx + \tilde{g}_j(y) = \sum_{l=0}^j -\frac{1}{j-l+1} a_{j-l,l}^y x^{j-l+1} y^l + \tilde{g}_j(y). \tag{65}$$

Integrating the second equation in (64),

$$\tilde{\psi}_j = \int \tilde{v}_j^x(x, y)dy + \tilde{f}_j(x) = \sum_{l=0}^j \frac{1}{l+1} a_{j-l,l}^x x^{j-l} y^{l+1} + \tilde{f}_j(x). \tag{66}$$

Subtracting (65) and (66), rearranging the summation indices, and incorporating the divergence-free conditions (63), we arrive at

$$\tilde{f}_j(x) - \tilde{g}_j(y) = -\frac{1}{j+1} a_{j,0}^y x^{j+1} - \frac{1}{j+1} a_{0,j}^x y^{j+1}. \tag{67}$$

Therefore, we conclude that a stream function $\tilde{\psi}_j \in \tilde{P}_{j+1}(K)$ exists for any divergence-free vector $\tilde{\mathbf{v}}_j \in (\tilde{P}_j(K))^2$, its functional form given by:

$$\tilde{\psi}_j(x, y) = \sum_{l=0}^j \frac{1}{l+1} a_{j-l,l}^x x^{j-l} y^{l+1} - \frac{1}{j+1} a_{j,0}^y x^{j+1}. \tag{68}$$

The stream function for the velocity field $\mathbf{v} \in RT_k^0(K)$ is simply the sum of the stream functions given by (68):

$$\psi_{RT_k^0}(x, y) = \sum_{j=0}^k \tilde{\psi}_j(x, y), \tag{69}$$

which indeed belongs to $P_{k+1}(K)$.

4.1.2 Brezzi-Douglas-Marini Spaces

We recall that the spaces $BDM_k(K)$ and $RT_k(K)$ contain the same divergence-free functions, that is, $BDM_k^0(K) \equiv RT_k^0(K)$. Therefore, the form of the stream function is identical:

$$\psi_{BDM_k^0}(x, y) = \psi_{RT_k^0}(x, y), \tag{70}$$

defined by (68) and (69).

4.2 Stream Functions on Rectangles

4.2.1 Raviart-Thomas Spaces

We recall the Raviart-Thomas space on the reference square:

$$RT_{[k]}(K) = (Q_k(K))^2 \oplus \mathbf{x}Q_k(K) = P_{k+1,k}(K) \times P_{k,k+1}(K) \\ = \left\{ \mathbf{v}(x, y) : \begin{bmatrix} v^x(x, y) \\ v^y(x, y) \end{bmatrix} = \begin{bmatrix} \sum_{i=0}^{k+1} \sum_{j=0}^k a_{i,j}^x x^i y^j \\ \sum_{i=0}^k \sum_{j=0}^{k+1} a_{i,j}^y x^i y^j \end{bmatrix} \right\}. \tag{71}$$

We impose the necessary condition of zero divergence, so that $\mathbf{v} \in RT^0_{[k]}(K)$:

$$\operatorname{div} \mathbf{v} = \sum_{i=1}^{k+1} \sum_{j=0}^k i a_{i,j}^x x^{i-1} y^j + \sum_{i=0}^k \sum_{j=1}^{k+1} j a_{i,j}^y x^i y^{j-1} = 0. \tag{72}$$

Rearranging the indices, we have

$$\sum_{i=0}^k \sum_{j=0}^k (i + 1) a_{i+1,j}^x x^i y^j = - \sum_{i=0}^k \sum_{j=0}^k (j + 1) a_{i,j+1}^y x^i y^j. \tag{73}$$

The following conditions must be satisfied for this relation to hold for any (x, y) :

$$(i + 1) a_{i+1,j}^x = -(j + 1) a_{i,j+1}^y \quad \text{for } i = 0, \dots, k, \quad j = 0, \dots, k. \tag{74}$$

Integrating the equations defining the stream function: $\tilde{v}_j \in (\tilde{P}_j(K))^2$:

$$\frac{\partial \psi}{\partial x} = -v^y(x, y), \quad \frac{\partial \psi}{\partial y} = v^x(x, y), \tag{75}$$

we obtain

$$\psi = - \int v^y(x, y) dx + g(y) = \sum_{i=0}^k \sum_{j=0}^{k+1} -\frac{1}{i+1} a_{i,j}^y x^{i+1} y^j + g(y), \tag{76}$$

$$\psi = \int v^x(x, y) dy + f(x) = \sum_{i=0}^{k+1} \sum_{j=0}^k \frac{1}{j+1} a_{i,j}^x x^i y^{j+1} + f(x). \tag{77}$$

Subtracting (76) and (77) and incorporating the divergence-free conditions (74):

$$f(x) - g(y) = - \sum_{i=0}^k \frac{1}{i+1} a_{i,0}^y x^{i+1} - \sum_{j=0}^k \frac{1}{j+1} a_{0,j}^x y^{j+1}. \tag{78}$$

Therefore, we conclude that a stream function $\psi \in Q_{k+1}(K)$ exists for any vector $\mathbf{v} \in RT^0_{[k]}(K)$, and its functional form is given by:

$$\psi(x, y) = \sum_{i=0}^{k+1} \sum_{j=0}^k \frac{1}{j+1} a_{i,j}^x x^i y^{j+1} - \sum_{i=0}^k \frac{1}{i+1} a_{i,0}^y x^{i+1}. \tag{79}$$

4.2.2 Brezzi-Douglas-Marini Spaces

Recall the space $BDM_{[k]}(K)$ defined on the reference square as:

$$BDM_{[k]}(K) = (P_k(K))^2 \oplus \operatorname{curl}(x^{k+1}y) \oplus \operatorname{curl}(xy^{k+1}). \tag{80}$$

Since the curl-terms are automatically divergence-free, they do not introduce any additional constraints. Therefore, the stream function of any function belonging to $BDM^0_{[k]}(K)$ can be constructed immediately:

$$\psi_{BDM^0_{[k]}}(x, y) = \psi_{RT^0_k}(x, y) + b_1 x^{k+1} y + b_2 x y^{k+1}, \tag{81}$$

where $\psi_{RT^0_k}$ is defined by (68) and (69).

5 Time-of-Flight

Mapping elements from physical space to a reference element and the use of the stream function allows one to efficiently compute the streamline and, in particular, the exit point. However, one crucial ingredient of streamline simulation is the accurate calculation of the travel time (or time-of-flight) along a streamline. Let \mathcal{L} be a streamline traversing an element from an entry point \mathbf{x}_0 to an exit point \mathbf{x}_f . The time-of-flight is defined as

$$\tau := \int_{\mathcal{L}} \frac{1}{|\mathbf{u}(s)|} ds, \tag{82}$$

where s is the arclength, or distance along the streamline.

One must be able to evaluate the integral in (82) in reference space (see Fig. 3). Simply substituting the velocity \mathbf{u} by its inverse Piola transform $\hat{\mathbf{u}}$ and evaluating the integral on the reference element yields an incorrect time-of-flight. To find the expression of the travel time as an integral evaluated on the reference space we need an appropriate *time mapping* between physical and reference configurations. A streamline satisfies the following equations in physical and reference space, respectively:

$$\frac{d\mathbf{x}}{dt} = \mathbf{u}(\mathbf{x}), \quad \frac{d\hat{\mathbf{x}}}{d\hat{t}} = \hat{\mathbf{u}}(\hat{\mathbf{x}}). \tag{83}$$

We recall the following relations:

$$d\mathbf{x} = \mathbf{D}(\hat{\mathbf{x}})d\hat{\mathbf{x}}, \tag{84}$$

$$\mathbf{u}(\mathbf{x}) = \frac{1}{J(\hat{\mathbf{x}})}\mathbf{D}(\hat{\mathbf{x}})\hat{\mathbf{u}}(\hat{\mathbf{x}}). \tag{85}$$

Using these expressions in (83), one immediately obtains the relation between t and \hat{t} :

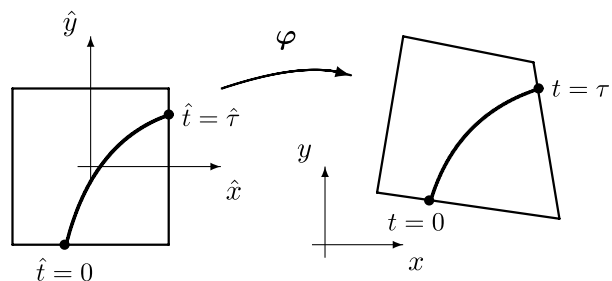
$$dt = J(\hat{\mathbf{x}})d\hat{t}. \tag{86}$$

Therefore, the *exact* expression of the time-of-flight as an integral on reference space is:

$$\tau = \int_{\hat{\mathcal{L}}} \frac{1}{|\hat{\mathbf{u}}(\hat{s})|} J(\hat{s}) d\hat{s}, \tag{87}$$

where \hat{s} is the arclength coordinate along the map of the streamline $\hat{\mathcal{L}}$ on the reference element.

Fig. 3 Transformation of the time-of-flight from the reference element to physical space



Remark For affine elements, the Jacobian of the transformation is constant and can be taken out of the integral. For distorted quadrilateral elements, however, the Jacobian varies inside the element and must be explicitly included in the integrand. Taking an approximate constant value of the Jacobian (for example, evaluated at the element center [34]) can lead to erroneous travel time predictions [20, 21].

6 Representative Simulations

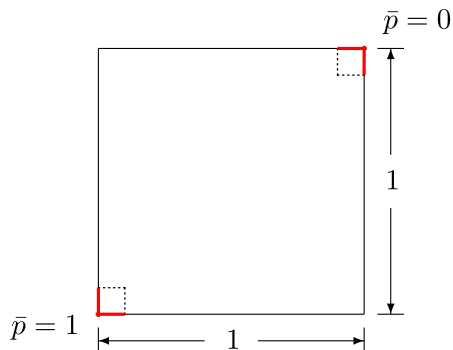
In this section we illustrate the performance of the proposed tracing strategy and assess the potential benefit of tracing streamlines based on high-order accurate velocity spaces. We restrict our attention to velocity spaces for which the associated pressure space is constant within each element. This design condition—driven by practical considerations in the area of groundwater flow and petroleum reservoir simulation—limits the choice of velocity spaces to the lowest-order Raviart-Thomas space (RT_0) and the Brezzi-Douglas-Marini space of order 1 (BDM_1). It is important to emphasize that, given a pressure-velocity solution to the flow problem (18)–(19) based on a particular discretization scheme (RT_0 or BDM_1), the streamlines and time-of-flight are *exact* (to be precise, they are computed with arbitrary accuracy). The specific functional forms of the velocity field, the stream function and the shape functions for RT_0 and BDM_1 elements on triangular and quadrilateral elements, along with algorithmic details, are given in a separate publication [26].

6.1 Robustness to Grid Distorsion

We study the behavior of low-order RT_0 and high-order BDM_1 streamline tracing in terms of accuracy and robustness to grid distortion. For this purpose, we consider a unit square flow domain $[0, 1] \times [0, 1]$, with isotropic, homogeneous permeability equal to one (see Fig. 4). The bottom-left corner of the domain is set at constant unit pressure, and the top-right corner at constant zero pressure. The rest of the boundary acts as a no-flow boundary. Therefore, the flow is from the bottom-left corner to the top-right corner. We solve the flow problem and trace streamlines using RT_0 and BDM_1 elements on a variety of quadrilateral and triangular grids:

1. A 10×10 Cartesian grid.
2. A *Chevron* grid, formed by keeping the vertical lines of the Cartesian grid and reorienting the horizontal edges to obtain a Chevron-like pattern.

Fig. 4 Sketch of the flow domain and boundary conditions for the diagonal flow problem



3. A *random* grid, created by a random relocation of the Cartesian grid nodes; the magnitude of node shifts is restricted to ensure that all elements are convex.
4. A *skewed* grid, obtained from a diagonal distortion of the Cartesian grid.

All four grids have 100 elements. Four triangular grids are created from these quadrilateral grids by splitting each quadrilateral element into two triangles. By construction, the triangular grids have twice as many elements as the quadrilateral grids: they are all composed of 200 elements.

Seven streamlines are traced on every grid and for each type of discretization. These streamlines are launched from equally spaced points along the diagonal of the square domain. In Fig. 5 we show the streamlines traced using the RT_0 and BDM_1 discretizations for all four quadrilateral grids. In Fig. 6 we plot the streamlines traced on the respective triangular grids.

The overall observation from these numerical examples is that the streamlines computed with an RT_0 approximation of the velocity are strongly influenced by grid distortion, while the BDM_1 approximation displays much less sensitivity to the choice of the grid. Specifically, we note the following:

1. RT_0 streamlines are particularly deficient for the quadrilateral Chevron grid (Fig. 5, second row). For example, the center streamline should be a straight line from the bottom-left corner to the top-right corner. The RT_0 approximation produces a highly skewed streamline, whereas the BDM_1 discretization results in a streamline trace that is almost straight and ends at the vertex of the corner blocks.
2. In the case of the quadrilateral skewed grid (Fig. 5, fourth row), RT_0 streamlines are missing their natural curvature, while BDM_1 streamlines show proper convexity.
3. An notorious deficiency is present in the streamlines computed with RT_0 on triangular grids. For this element type, the velocity field is constant over each element. Since boundaries are impervious (no-flow), elements in contact with the boundary necessarily have RT_0 streamlines that are parallel to the boundary. This built-in constraint results in jagged, nonphysical streamlines. The phenomenon is obvious in the traces of the longest streamlines, especially near the corner blocks. The results on a skewed grid (Fig. 6, fourth row) illustrate this undesirable effect particularly well. On the other hand, the BDM_1 approximation allows for the velocity field to vary within each element and, as a consequence, streamlines can bend even along boundary blocks. This added flexibility is reflected in the vastly improved behavior of the streamline traces, which are much more physical and much less grid-dependent.

To quantify the apparent increased accuracy and robustness of the streamlines based on the higher-order velocity approximation, we compute the error in the time-of-flight for each of the seven streamlines. Reference values are obtained using a 100×100 Cartesian grid with a BDM_1 discretization.

In Table 1 we report, for each grid and type of discretization, the time-of-flight error for the streamline passing through the point of coordinates $(x, y) = (\frac{3}{14}, \frac{11}{14})$. This streamline was chosen arbitrarily and was found to be representative of the results observed with the six other streamlines. We note the following observations:

1. We observe a consistent and significant reduction of the time-of-flight errors when using the higher-order BDM_1 approximation rather than the low-order RT_0 approximation.
2. The variability of the BDM_1 time-of-flight error is much smaller than that of RT_0 , confirming the robustness of the BDM_1 -based streamline tracing with respect to grid distortion.

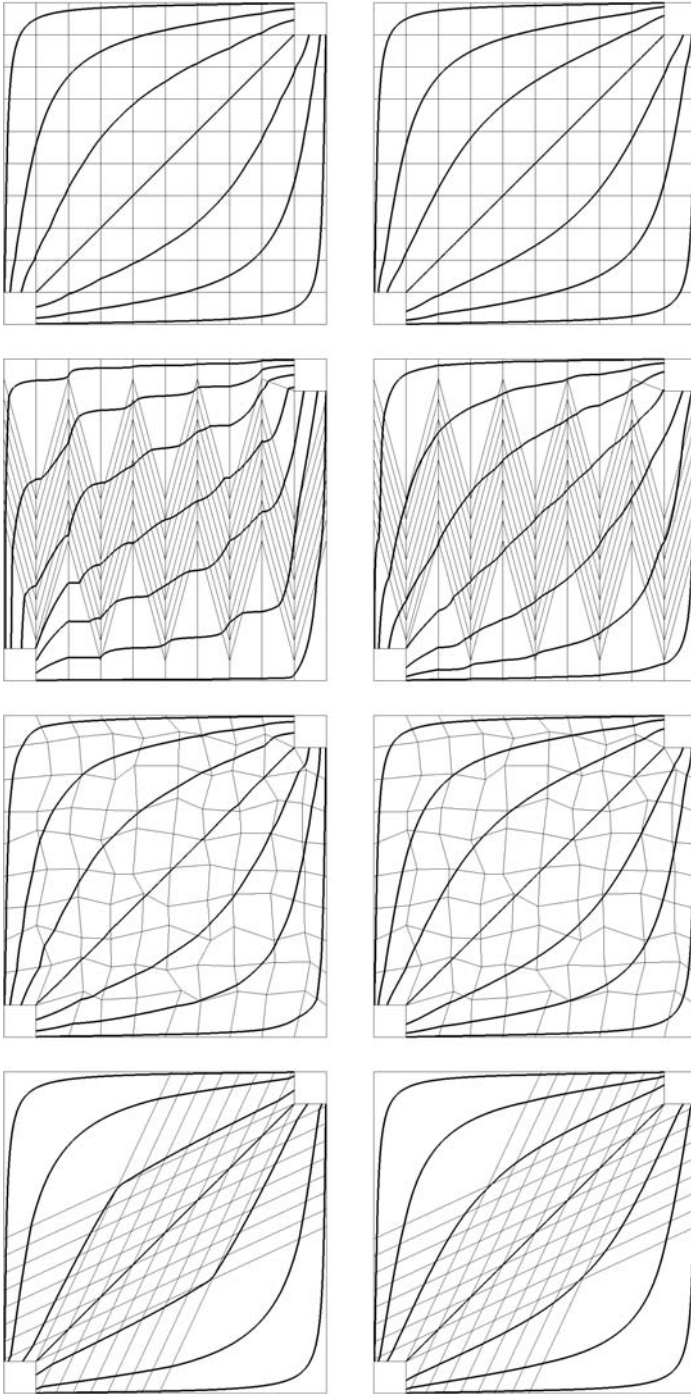


Fig. 5 RT_0 (left) and BDM_1 (right) streamlines on quadrilateral grids. From top to bottom: Cartesian, Chevron, random, and skewed grids

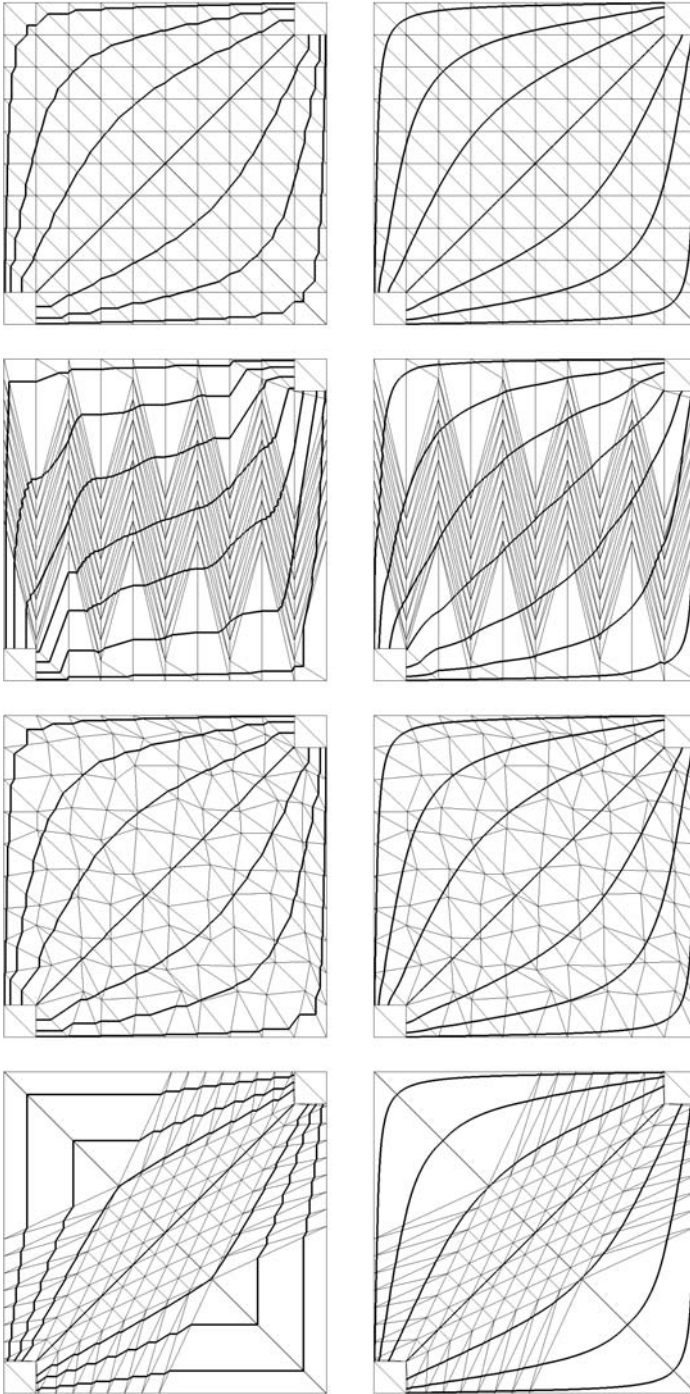
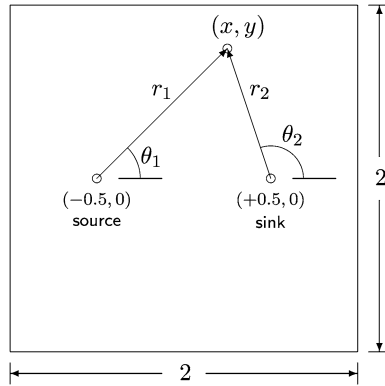


Fig. 6 RT_0 (left) and BDM_1 (right) streamlines on triangular grids. From top to bottom: Cartesian, Chevron, random, and skewed grids

Table 1 Time-of-flight error for the streamline passing through the point $(x, y) = (\frac{3}{14}, \frac{11}{14})$

Element type	Discretization	Cartesian	Chevron	Random	Skewed
Triangle	RT_0^0	16.89%	35.53%	18.01%	17.83%
	BDM_1^0	6.13%	7.50%	6.11%	7.58%
Quadrilateral	RT_0^0	16.69%	35.77%	17.79%	47.69%
	BDM_1^0	3.49%	4.95%	3.45%	2.72%

Fig. 7 Sketch of the flow domain and boundary conditions for the source-sink pair flow problem



On a given grid, the solution of the flow problem is more computationally expensive using BDM_1 elements than RT_0 elements, since the BDM_1 approximation involves roughly twice as many velocity unknowns. An interesting and legitimate question is whether the accuracy of BDM_1 -based streamline tracing is still higher than that of RT_0 -based tracing for the same computational cost. This and other related questions are addressed at length in a separate publication [26].

6.2 Unstructured Grids

We now investigate the applicability of the method on truly unstructured grids. We use a problem for which an analytical solution exists. The analytical problem consists of a source-sink pair in an infinite, homogeneous medium of unit permeability. The source—of unit strength—is located at $(-\frac{1}{2}, 0)$ and the sink at $(+\frac{1}{2}, 0)$. For an arbitrary point on the (x, y) -plane, we define the following variables: r_1, r_2 are the distances to the source and sink, respectively, and θ_1, θ_2 are the corresponding angles with the x -axis (see Fig. 7):

$$\begin{aligned}
 r_1 &= \left(\left(x + \frac{1}{2} \right)^2 + y^2 \right)^{1/2}, & \theta_1 &= \tan^{-1} \left(\frac{y}{x + \frac{1}{2}} \right), \\
 r_2 &= \left(\left(x - \frac{1}{2} \right)^2 + y^2 \right)^{1/2}, & \theta_2 &= \tan^{-1} \left(\frac{y}{x - \frac{1}{2}} \right).
 \end{aligned}
 \tag{88}$$

The analytical solution can then be expressed in terms of the flow potential (in this case, equal to the pressure),

$$p = \ln r_1 - \ln r_2,
 \tag{89}$$

Table 2 Pressure and velocity errors and convergence rates (L^2 norm) for the refinement study on unstructured grids

Method	h	$\ p - p_h\ _{L^2}$	$\ \mathbf{u} - \mathbf{u}_h\ _{L^2}$
RT_0	0.5	1.70E-01	2.13E+00
	0.25	8.62E-02	1.25E+00
	0.125	4.32E-02	6.56E-01
	Rate	0.995	0.935
BDM_1	0.5	1.66E-01	6.31E-01
	0.25	8.55E-02	1.91E-01
	0.125	4.32E-02	5.26E-02
	Rate	0.987	1.860

or the stream function,

$$\psi = \theta_1 - \theta_2. \quad (90)$$

We set up our numerical simulations by imposing prescribed-pressure boundary conditions at the outer boundary of the domain $\Omega_0 = [-1, 1] \times [-1, 1]$, as well as at the inner boundaries, which are squares around the source and sink:

$$\begin{aligned} \omega_1 &= \left[-\frac{1}{2} - \varepsilon, -\frac{1}{2} + \varepsilon \right] \times [-\varepsilon, \varepsilon], \\ \omega_2 &= \left[\frac{1}{2} - \varepsilon, \frac{1}{2} + \varepsilon \right] \times [-\varepsilon, \varepsilon], \end{aligned} \quad (91)$$

with $\varepsilon = 0.1$. The domain in which the flow problem is solved is $\Omega = \Omega_0 \setminus \{\omega_1 \cup \omega_2\}$.

In Fig. 8 we compare the numerical streamlines obtained by the RT_0 and BDM_1 discretizations on a sequence of increasingly refined fully unstructured grids. The analytical streamlines are also shown for reference. Clearly, the visual comparison is very favorable for the higher-order streamlines, as they coincide almost exactly with the analytical streamlines, even on coarse grids.

Table 2 reports the errors and convergence rates of the pressure and velocity fields (in the L^2 norm). These numerical results simply confirm the theoretical estimates [10, 35] that predict a first-order convergence of the RT_0 velocity field, a second-order convergence for the BDM_1 velocity field and a first-order convergence of the pressure field for both spaces.

Quantification of the behavior of the time-of-flight as the grid is refined is more subtle. The time-of-flight error does not display a consistent convergence rate, common to all streamlines. We observed that the convergence properties in terms of time-of-flight were strongly dependent on the streamline chosen and did not necessarily reach an asymptotic value. This dependency of the tracing accuracy to the location of the streamline was already observed in [25].

Although the convergence rates in terms of time-of-flight are rather unpredictable, it was found that the BDM_1 streamlines are always significantly more accurate than the ones obtained with an RT_0 approximation, both in terms of location and time-of-flight.

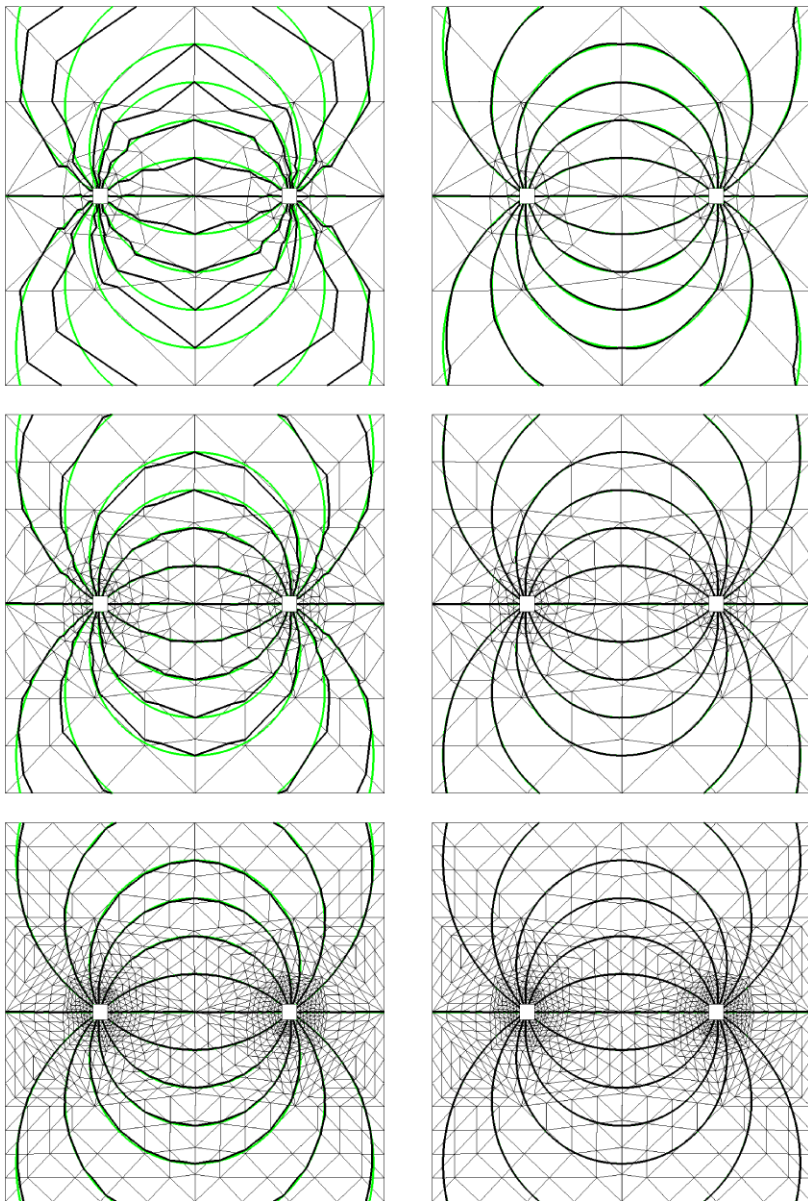


Fig. 8 (Color online) Comparison of the numerical (*black*) and analytical (*green*) streamlines on a sequence of increasingly refined unstructured grids. *Left column: RT_0^0 space. Right column: BDM_1^0 space*

7 Conclusions

We have presented a unified formulation for streamline tracing on unstructured grids. The formulation has three key ingredients: (1) the use of the Piola transform to map the velocity between physical space and a reference configuration; (2) the choice of an appropriate approximation of the velocity field; and (3) the use of the stream function to define the

streamline location. One of the main contributions of this paper is the identification of velocity spaces that induce a stream function. Such velocity spaces are taken from the theory of mixed finite element methods. In this way, not only do we justify theoretically the low-order tracing algorithms currently in use (Pollock's method [33]), but we also show how to choose velocity approximations for higher-order tracing on general triangular and quadrilateral grids. Moreover, we derive the precise functional form of the stream function for each class of velocity spaces, which can be seen as a constructive proof of the existence of the stream function for the velocity spaces of choice.

We have illustrated the performance of the proposed streamline tracing framework for velocity spaces that are compatible with a piecewise constant—discontinuous—pressure solution: the lowest-order Raviart-Thomas space (RT_0) and the Brezzi-Douglas-Marini space of order one (BDM_1). We conclude that BDM_1 -based tracing is much more accurate (smaller error in the time-of-flight) and robust (less sensitive to grid distortion) than RT_0 -based tracing. The algorithmic details of the formulation and a more thorough investigation of the numerical performance is presented in another paper [26].

The developments presented here are restricted to two-dimensional problems. Although conceptually possible, the extension to three dimensions requires the use of dual stream functions [5] and it is not straightforward. A different approach, based on corner-velocity interpolation, has been proposed recently [20]. The present paper, however, serves as a motivation to evaluate the accuracy and robustness of streamline tracing based on a higher-order velocity approximation in three dimensions [28, 29].

References

1. Ackerer, P., Mosé, R., Siegel, P., Chavent, G.: Application of the mixed hybrid finite element approximation in a groundwater flow model: Luxury or necessity? Reply to the Comment by C. Cordes and W. Kinzelbach. *Water Resour. Res.* **32**(6), 1911–1913 (1996)
2. Aziz, K., Settari, A.: *Petroleum Reservoir Simulation*. Elsevier, Amsterdam (1979)
3. Babuška, I.: The finite element method with Lagrangian multipliers. *Numer. Math.* **20**, 179–192 (1973)
4. Batycky, R.P., Blunt, M.J., Thiele, M.R.: A 3D field-scale streamline-based reservoir simulator. *SPE Reserv. Eng.* **11**(4), 246–254 (1997)
5. Bear, J.: *Dynamics of Fluids in Porous Media*. Environmental Science Series. Elsevier, Amsterdam (1972). Reprinted with corrections, Dover, New York (1988)
6. Bratvedt, F., Bratvedt, K., Buchholz, C.F., Gimse, T., Holden, H., Holden, L., Risebro, N.H.: Frontline and Frontsim, two full scale, two-phase, black oil reservoir simulators based on front tracking. *Surv. Math. Ind.* **3**, 185–215 (1993)
7. Brenner, S.C., Scott, L.R.: *The Mathematical Theory of Finite Element Methods*. Texts in Applied Mathematics, vol. 15. Springer, New York (1994)
8. Brezzi, F.: On the existence, uniqueness and approximation of saddle point problems arising from Lagrange multipliers. *RAIRO Anal. Numér.* **8**, 129–151 (1974)
9. Brezzi, F., Fortin, M.: *Mixed and Hybrid Finite Element Methods*. Springer Series in Computational Mathematics, vol. 15. Springer, New York (1991)
10. Brezzi, F., Douglas, J. Jr., Marini, L.D.: Two families of mixed finite elements for second order elliptic problems. *Numer. Math.* **47**, 217–235 (1985)
11. Brezzi, F., Douglas, J. Jr., Duran, R., Fortin, M.: Mixed finite elements for second order elliptic problems in three variables. *Numer. Math.* **51**, 237–250 (1987)
12. Cai, Z., Douglas, J. Jr., Park, M.: Development and analysis of higher order finite volume methods over rectangles for elliptic equations. *Adv. Comput. Math.* **19**, 3–33 (2003)
13. Chavent, G., Jaffré, J.: *Mathematical Models and Finite Elements for Reservoir Simulation*. Studies in Mathematics and Its Applications, vol. 17. Elsevier, Amsterdam (1986)
14. Chen, Z., Ewing, R.E.: Comparison of various formulations of three-phase flow in porous media. *J. Comput. Phys.* **132**, 362–373 (1997)
15. Cordes, C., Kinzelbach, W.: Continuous groundwater velocity fields and path lines in linear, bilinear, and trilinear finite elements. *Water Resour. Res.* **28**(11), 2903–2911 (1992)

16. Cordes, C., Kinzelbach, W.: Comment on “Application of the mixed hybrid finite element approximation in a groundwater flow model: Luxury or necessity?” by R. Mosé, P. Siegel, P. Ackerer, and G. Chavent. *Water Resour. Res.* **32**(6), 1905–1909 (1996)
17. Durlafsky, L.J.: Accuracy of mixed and control volume finite element approximations to Darcy velocity and related quantities. *Water Resour. Res.* **30**(4), 965–973 (1994)
18. Feng, D., Wang, X.M., Cai, W.L., Shi, J.: A mass conservative flow field visualization method. *Comput. Graph.* **21**(6), 749–756 (1997)
19. Guadagnini, A., Sánchez-Vila, X., Riva, M., De Simoni, M.: Mean travel time of conservative solutes in randomly heterogeneous unbounded domains under mean uniform flow. *Water Resour. Res.* **39**(3), 1050 (2003). doi:[10.1029/2002WR001811](https://doi.org/10.1029/2002WR001811)
20. Hægland, H., Dahle, H.K., Eigestad, G.T., Lie, K.A., Aavatsmark, I.: Improved streamlines and time-of-flight for streamline simulation on irregular grids. *Adv. Water Resour.* **30**(4), 1027–1045 (2007). doi:[10.1016/j.advwatres.2006.09.002](https://doi.org/10.1016/j.advwatres.2006.09.002)
21. Jimenez, E., Sabir, K., Datta-Gupta, A., King, M.J.: Spatial error and convergence in streamline simulation. *SPE Reserv. Eval. Eng.* **10**(3), 221–232 (2007)
22. Kaasschieter, E.F.: Mixed finite elements for accurate particle tracking in saturated groundwater flow. *Adv. Water Resour.* **18**(5), 277–294 (1995)
23. King, M.J., Datta-Gupta, A.: Streamline simulation: A current perspective. *In Situ* **22**(1), 91–140 (1998)
24. Marsden, J.E., Hughes, T.J.R.: *Mathematical Foundations of Elasticity*. Prentice-Hall, Englewood Cliffs (1983). Reprinted with corrections, Dover, New York (1994)
25. Matringe, S.F., Gerritsen, M.G.: On accurate tracing of streamlines. In: *SPE Annual Technical Conference and Exhibition, Houston, TX (SPE 89920)* (2004)
26. Matringe, S.F., Juanes, R., Tchelepi, H.A.: Robust streamline tracing for the simulation of porous media flow on general triangular and quadrilateral grids. *J. Comput. Phys.* **219**, 992–1012 (2006). doi:[10.1016/j.jcp.2006.07.004](https://doi.org/10.1016/j.jcp.2006.07.004)
27. Matringe, S.F., Juanes, R., Tchelepi, H.A.: Tracing streamlines on unstructured grids from finite volume discretizations. In: *SPE Annual Technical Conference and Exhibition, San Antonio, TX (SPE 103295)* (2006). To appear in *Soc. Pet. Eng. J.*
28. Matringe, S.F., Juanes, R., Tchelepi, H.A.: Mixed finite element and related control volume discretizations for reservoir simulation on three-dimensional unstructured grids. In: *SPE Reservoir Simulation Symposium, Houston, TX (SPE 106117)* (2007)
29. Matringe, S.F., Juanes, R., Tchelepi, H.A.: A new mixed finite element on hexahedra that reduces to a cell-centered finite difference method. *Numer. Math.* (2008, submitted)
30. Matringe, S.F., Juanes, R., Tchelepi, H.A.: Streamline tracing on general triangular or quadrilateral grids. *Soc. Pet. Eng. J.* **12**(2), 217–223 (2007). doi:[10.2118/96411-PA](https://doi.org/10.2118/96411-PA)
31. Mosé, R., Siegel, P., Ackerer, P., Chavent, G.: Application of the mixed hybrid finite element approximation in a groundwater flow model: Luxury or necessity? *Water Resour. Res.* **30**(11), 3001–3012 (1994)
32. Nedelec, J.C.: Mixed finite elements in \mathbb{R}^3 . *Numer. Math.* **35**, 315–341 (1980)
33. Pollock, D.W.: Semianalytical computation of path lines for finite difference models. *Ground Water*. **26**, 743–750 (1988)
34. Prevost, M., Edwards, M.G., Blunt, M.J.: Streamline tracing on curvilinear structured and unstructured grids. *Soc. Pet. Eng. J.* **7**(2), 139–148 (2002)
35. Raviart, P.A., Thomas, J.M.: A mixed finite element method for second order elliptic problems. In: Galligani, I., Magenes, E. (eds.) *Mathematical Aspects of the Finite Element Method*. Lecture Notes in Mathematics, vol. 606, pp. 292–315. Springer, New York (1977)
36. Russell, T.F., Wheeler, M.F.: Finite element and finite difference methods for continuous flows in porous media. In: Ewing, R.E. (ed.) *The Mathematics of Reservoir Simulation*, pp. 35–106. SIAM, Philadelphia (1983)
37. Weiser, A., Wheeler, M.F.: On convergence of block-centered finite differences for elliptic problems. *SIAM J. Numer. Anal.* **25**(2), 351–375 (1988)
38. Wheeler, M.F., Yotov, I.: A multipoint flux mixed finite element method. *SIAM J. Numer. Anal.* **44**(5), 2082–2106 (2006)